

Seasonal coupling of canopy structure and function in African tropical forests and its environmental controls

KAIYU GUAN,^{1,†} ADAM WOLF,² DAVID MEDVIGY,³ KELLY K. CAYLOR,¹ MING PAN,¹ AND ERIC F. WOOD¹

¹*Department of Civil and Environmental Engineering, Princeton University, Princeton, New Jersey 08544 USA*

²*Department of Ecology and Evolutionary Biology, Princeton University, Princeton, New Jersey 08544 USA*

³*Department of Geosciences, Princeton University, Princeton, New Jersey 08544 USA*

Citation: Guan, K., A. Wolf, D. Medvigy, K. K. Caylor, M. Pan, and E. F. Wood. 2013. Seasonal coupling of canopy structure and function in African tropical forests and its environmental controls. *Ecosphere* 4(3):35. <http://dx.doi.org/10.1890/ES12-00232.1>

Abstract. Tropical forests provide important ecosystem services in maintaining biodiversity, sequestering carbon and regulating climate regionally and globally. Climate triggers the seasonal transitions of vegetation structure and function in tropical forests. In turn, the seasonal cycles of structure and function in tropical forests feed back to the climate system through the control of land-atmosphere exchange of carbon, water and energy fluxes. Large uncertainties exist in the carbon and water budgets of tropical forests, and environmental controls on phenology are among the least understood factors. Although field studies have identified patterns in the environmental controls on local-scale species-level phenology in the tropics, there is little consensus on large-scale top-down environmental controls on whole-ecosystem seasonality. In this paper, we use both optical and microwave remote sensing to investigate the seasonality of vegetation canopy structure and function in three distinct tropical African forest types, and identify environmental triggers or controls of their variability. For most tropical forests that have a closed canopy and high leaf biomass, optical remote sensing (e.g., vegetation indices) captures canopy photosynthetic capacity (i.e., canopy function), while small-wavelength microwave remote sensing characterizes the leaf biomass and leaf water content of the upper canopy (i.e., canopy structure). Our results reveal a strong coupling of canopy structure with canopy function in the tropical deciduous forests and woody savannas, and their seasonalities are both controlled by precipitation rather than solar radiation. By contrast, tropical evergreen forests in Africa exhibit a decoupling of canopy structure from canopy function revealed by different sensors: canopy photosynthetic capacity shown by the optical remote sensing is linked to the seasonal variation of precipitation, while microwave remote sensing captures semi-annual leaf-flushing that is synchronous with peak insolation intensity at the top of the atmosphere, which is bimodal. The differential coupling of canopy structure and function in tropical forests observed from remote sensing highlights differences inherent in distinct vegetation types within the tropics that may originate in the different life histories of their respective floras. This satellite-based finding encourages more field-based studies to clarify the interpretation of these large scale patterns.

Key words: Africa; Enhanced Vegetation Index (EVI); microwave remote sensing; optical remote sensing; phenology; Scatterometer backscattering coefficient; tropical forests.

Received 30 July 2012; **revised** 24 January 2013; **accepted** 25 January 2013; **final version received** 25 February 2013;
published 18 March 2013. Corresponding Editor: H. A. Epstein.

Copyright: © 2013 Guan et al. This is an open-access article distributed under the terms of the Creative Commons Attribution License, which permits unrestricted use, distribution, and reproduction in any medium, provided the original author and source are credited. <http://creativecommons.org/licenses/by/3.0/>

† **E-mail:** kguan@princeton.edu

INTRODUCTION

Tropical forests have the highest terrestrial biodiversity on the Earth (Dirzo and Raven 2003), contain around 25% of the carbon in the terrestrial biosphere (Bonan 2008), and intact tropical forests collectively possess the largest annual rate of carbon sequestration among all terrestrial ecosystems (Pan et al. 2011). Tropical forests are also strongly coupled to the climate system, both responding to climate variability (Nemani et al. 2003) and regulating the climate system through physical, chemical, and biological processes that affect planetary boundary layer dynamics, the hydrologic cycle, and atmospheric composition (Bonan 2008, Richardson et al. 2013). Nevertheless, many aspects of tropical forest dynamics remain poorly understood. The estimated size of the tropical forest carbon sink since 1990 is more uncertain than for any other forest biome (Pan et al. 2011), and models give a wide range of projections for the tropical forest response to climate change (Sitch et al. 2008). A particular gap in our understanding pertains to the seasonality, or phenology, of tropical forests (Saleska et al. 2009, van Schaik et al. 1993), which is exemplified by the lack of ground observation (Wright and van Schaik 1994) as well as the struggle to accurately simulate the seasonality of tropical forests by dynamic vegetation models (Kim et al. 2012). These uncertainties are likewise evident in the weak process level understanding of the seasonal variation in land-atmosphere exchange (Fisher et al. 2009).

The phenological development of tree species is characterized by distinct seasonal phases of bud burst, leaf flushing, flowering, senescence and dormancy (Calle et al. 2010). The timing of these events fulfills multiple objectives in a plant's life cycle, including matching resource demand with availability and synchronizing with pollinators (Yeang 2007a, Wright and van Schaik 1994), while working within the constraints imposed by environmental extremes (e.g., cold temperatures, water deficit, light limitation). Phenological changes in vegetation are also associated with seasonal variation in land-atmosphere gas exchange, including photosynthesis and transpiration, due to the dependence of these fluxes on leaf area and its physiology. For tropical species that occupy a weakly seasonal environ-

ment, the physical changes in canopy structure and physiological changes in canopy function are not necessarily synchronized in time and may have different top-down controls (Doughty and Goulden 2008, Huete et al. 2008). While there is a long history of studying rhythmic growth in individual tropical species (Hallé et al. 1978, Reich 1995), there remains a gap in the understanding of how leaf display is related seasonally to leaf photosynthesis, and what the large-scale controls of this synchrony are across a range of climates and vegetation types in the tropics. Hereafter, we refer to the canopy leaf biomass as "vegetation canopy structure", and the canopy photosynthetic activities as "vegetation canopy function".

It is widely thought that environmental cues trigger changes in leaf biomass (Hallé et al. 1978), though internal regulation of plants may play a role in highly aseasonal tree species (Reich 1995, Williams et al. 1997). In the tropics, the two most important environmental cues relate to radiation and water (van Schaik et al. 1993). In brief, where rainfall seasonality is pronounced, dry-season drought primarily constrains phenology (Reich and Borchert 1984); where water resources are ample, sunlight plays a more important role in triggering transitions in phenological phases (Wright and van Schaik 1994). However, the details of how these environmental constraints ultimately impact phenology are still controversial in tropical forests (van Schaik et al. 1993), and highly species-dependent (Williams et al. 1997).

For example, the impact of radiation has been hypothesized to be mediated either through daylength (Rivera and Borchert 2001, Rivera et al. 2002, Elliott et al. 2006, Williams et al. 2008), timing of sunrise or sunset (Borchert et al. 2005), or insolation thresholds (van Schaik et al. 1993, Wright and van Schaik 1994, Yeang 2007a, 2007b, Calle et al. 2009, 2010). The insolation threshold pertains to solar radiation intensity at the top of the atmosphere (i.e., shortwave downward radiation at the top of atmosphere, "SWTOA" hereafter). SWTOA has two peaks over the tropical equator on the equinoxes, and these two peaks in SWTOA coincide with semi-annual tropical forest flowering and leaf flushing found from field observations (Yeang 2007a, Wright and van Schaik 1994, Calle et al. 2009, 2010). Because SWTOA is related to the direct sunlight in the

clear sky at midday, which can be perceived by plants, it is proposed that SWTOA is a strong tropical phenology trigger. Mechanistic evidence for this hypothesis is provided by the finding that strong insolation plays a direct role in the transcription of genes that influence floral/leaf development (Jackson 2009). However, maximum SWTOA control on tropical leaf phenology has not been verified at large scales, mostly because no suitable measurements have been available. It is worth noting that SWTOA is different from shortwave radiation at the top of canopy (SWCNP), which is diminished from SWTOA by clouds and aerosols in the atmosphere.

Other radiation-related hypotheses have been proposed and tested in the past. The daylength hypothesis fails to explain the seasonality of evergreen forests in the tropical equator since there is little variation in day-length at equator regions (Renner 2007). The hypothesis of timing of sunrise or sunset proposes that the seasonal shifts in these events as a result of the Earth's axial tilt and its elliptic orbit trigger the synchronous flowering/leaf-flushing at the equator (Borchert et al. 2005). The relevance for this hypothesis in the tropics has been questioned, because it would require plants to sense subtle cyclical shifts (30 minutes over the course of a year) that arise between solar time and an external reference chronometer time (Renner 2007, Yeang 2007a, 2007b).

The water-related hypotheses are also controversial because phenological patterns vary widely within the same species or among different species in tropical forests (Williams et al. 1997). Many tropical forests have well-established drought-adaptive mechanisms linking the seasonality of growth with the seasonality of water availability. These strategies include deploying deep roots to access soil water reserves, which potentially allows them to grow in the dry season (Nepstad et al. 1994, Dawson 1996, Borchert 1998, Meir et al. 2009, Markowitz et al. 2010), or by timing leaf flushing to precede the onset of the rainy season (Williams et al. 2008).

Remote sensing has provided unique opportunities to monitor large-scale temporally-continuous vegetation dynamics (Chambers et al. 2007). Vegetation Indices (VI) from optical remote sensing have been widely used in

vegetation monitoring (Tucker et al. 2008), typically using some variation of a ratio or difference between reflectance in the red (R) and near-infrared (NIR), such as the Normalized Difference Vegetation Index: $NDVI = (NIR - R)/(NIR + R)$. In this study we used a related VI, the Enhanced Vegetation Index (EVI), which is in many ways similar to NDVI but includes a term that alleviates atmospheric effects of aerosols released in biomass burning (Huete et al. 2002). The difference in reflectance in R and NIR differentiates green vegetation from soil and non-photosynthetic vegetation. At the canopy level, EVI is linear to the fraction of absorbed photosynthetically active radiation (fAPAR), which is directly related to canopy photosynthetic capacity, but is not a reliable predictor of leaf area index or biomass, especially for vegetation with thick and closed canopy (Sellers 1985, 1987, 1992). This relationship can also be confounded by soil reflectivity in sparse canopies (Sellers 1987). At landscape scales, EVI is a composite variable influenced by leaf biochemical properties, canopy structure and vegetation fractions (Glenn et al. 2008, Guan et al. 2012). For closed, dense canopies with little soil contribution to reflectance, such as those in tropical forests, EVI has limited sensitivity to extremely high leaf biomass (esp. those in the tropical evergreen forests) (Doughty and Goulden 2008), and its variation can be attributed to changes in canopy photosynthetic capacity for these forests (Huete et al. 2008).

Microwave remote sensing (both passive radiometry and active radar) has gradually gained attention for vegetation monitoring during the past two decades (Waring et al. 1995, Hardin and Jackson 2003, Frolking et al. 2005, 2006, 2012). Microwave instruments are generally much less sensitive to atmospheric aerosols and moisture than optical sensors (Ulaby et al. 1982), and insensitive to seasonal variations in incoming solar radiation (Frolking et al. 2011). The energy in microwave backscattering from terrestrial landscapes is determined by surface dielectric properties, modulated by microwave frequency (or wavelength), polarization and viewing angle. The dielectric property of a landscape is strongly dependent on its liquid water content (Jensen 2000). Different microwave frequencies have been used for different purposes. Large micro-

wave wavelengths, such as P-band and L-band, have strong penetration capabilities through the whole crown layer of tropical forests, and the crown layer (mainly branches) and trunk are the major contribution of the observed backscatter. Thus they have been used to estimate total above ground biomass (Toan et al. 1992, Saatchi et al. 2011). As the frequency decreases, C-band and Ku-band capture more backscattering from leaf and twigs (leaf biomass) of the upper canopy of tropical forests (Toan et al. 1992, Waring et al. 1995). Past research has found that for sparse vegetation regions, such as grasslands and savannas, C-band and Ku-band backscattering observations require careful interpretation because soil moisture can modulate the signal (Jarlén et al. 2002). By contrast, in tropical evergreen forests, with closed canopies, C-band and Ku-band backscattering are more strongly related to leaf biomass dynamics, with limited contribution from soil moisture (Frolking et al. 2011). Another advantage of C-band and Ku-band is the high revisit frequency (daily or sub-daily) of the satellite platforms that carry these sensors. Nevertheless, despite these advantages, there are still relatively few studies applying these data for monitoring the dynamics of tropical forests (Frolking et al. 2011, 2012).

In this paper, we aim to use multiple remote sensing datasets from both optical and microwave platforms to assess the environmental controls on the seasonality of vegetation function and structure in African tropical forests by testing multiple hypotheses that have been proposed from field research. Tropical Africa contains 18% of global tropical forests by area, but has been understudied compared to the Neotropical and Asian tropical forest. The specific science questions we will address in this paper are: (1) What are the spatial and temporal patterns of vegetation phenology in African tropical evergreen forests, tropical deciduous forests and woody savannas? (2) What are the environmental controls that best explain the spatio-temporal patterns of the vegetation phenology in African tropics? We answer these questions by assessing the correlations between satellite-measured vegetation indices with precipitation, SWCNP, SWTOA, day-length and sunrise (or sunset) time.

MATERIALS AND METHODS

Data

We use two optical remote sensing datasets and two microwave scatterometer datasets for vegetation monitoring (Table 1, also see all the acronyms in Appendix A). Two optical remote sensing (ORS) datasets are NDVI from GIMMS (based on AVHRR) and EVI from MODIS (MOD13C1, Version 5), which have been widely used for regional and global vegetation applications (Huete et al. 2002, Tucker et al. 2008). Both AVHRR and MODIS sensors are polar-orbiting sun-synchronous satellites. EVI has improved performance over the traditionally-used NDVI, by addressing atmospheric effects as well as improving its sensitivity for high leaf biomass canopy (Huete et al. 2002). Two microwave remote sensing (MVRs) datasets are from QuikSCAT and ERS-1/-2. QuikSCAT is a Ku-band (13.4 GHz, or 2.1 cm wavelength) active radar with two rotating pencil beam antennas operating in H and V polarizations at an incidence angles of 55° and 46°. The Ku-band backscatter coefficient (called “Ku-dB” hereafter) product from QuikSCAT that we use combines ascending and descending overpass together for a daily composite (Long 2001), and since H-band and V-band have little difference for our analysis, V-band results are shown in the paper. ERS-1/-2 are C-band (5.3 GHz, or 5.7 cm wavelength, called “C-dB” hereafter) active radar instruments, and only V-band data are available (http://www.scp.byu.edu/docs/ERS_user_notes.html).

Satellite-gauge-merged precipitation dataset TRMM 3b42V6 (Huffman et al. 2007) and geostationary-satellite-based surface shortwave downward radiation (SWCNP) from NASA MEASUREs project are used (Ma and Pinker 2012). Calculation of insolation intensity at the top of atmosphere (SWTOA) follows the corresponding algorithm in NASA Atmosphere-Ocean Model GISS (<http://aom.giss.nasa.gov/SOLAR/SRLOCAT.FOR>).

Since both ORS and MVRs data contain random noise from various sources such as electronic noise and geometric positioning, an advanced smoothing scheme (Garcia 2010) was applied to aggregate all good-quality data into half-monthly level (the data filtering is done based on the data quality flags). This smoothing

Table 1. Datasets used in this study: variable fields, resolution and source.

Data product	Temporal resolution	Spatial resolution	Coverage	Reference†
Optical sensors				
GIMMS NDVI	half monthly	8 km	07/1981–12/2008	GIMMS ¹
MODIS EVI/NDVI	16 days	0.05° (~5 km)	02/2000–present	MOD13C1 ²
SEVERI LAI	daily	3~5 km	01/2007–present	SEVERI ³
Active scatterometers				
QuikSCAT Ku-dB	daily	25 km	07/1999–11/2009	QuikSCAT ⁴
ERS-1/2 C-dB	every 6 day	25 km	01/1992–01/2001	ERS-1/2 AMI ⁵
TRMM precipitation	daily	25 km	1998–present	TRMM 3b42V ⁶
Shortwave downward (SWD) radiation	daily	0.5° (~50 km)	1984–2007	MEaSUREs ⁷

† References are: 1, Tucker et al. (2003); 2, Solano et al. (2010); 3, García-Haro et al. (2008); 4, Long (2001); 5, http://www.scp-byu.edu/docs/ERS_user_notes.html; 6, Huffman et al. (2007); 7, Ma and Pinker (2012).

scheme is fully automated based on a penalized least squares method (Garcia 2010; see Appendix B: Fig. B1). We find that different smoothing approaches do not change the results or conclusions in this work. All the data were aggregated or interpolated to 0.1 degree (~10 km) and half-monthly. We only show the result of EVI for ORS, and Ku-dB for MVRS because EVI and Ku-dB are representative of ORS and MVRS performances. Results of other data can be found in the Appendix B.

Study area

This study focuses on the regions dominated by tropical evergreen forests (5° N–7° S in latitude and 10° E–30° E in longitude), tropical deciduous forests and woody savannas (regions northern of 5° N and southern of 7° S). We use the annual LAI mean value of 1.0 (from SEVERI, see Table 1) as a threshold to delineate the regions of tropical forests with other ecosystems, which is generally consistent with land cover classifications from the GLC2000 Africa product (Mayaux et al. 2003, also see Fig. 1).

Methods

1. *Power spectra and phase analysis*.—Fourier transforms were used to extract the power spectra at the per-pixel level. Each time series was normalized by its standard deviation before the Fourier transform for the purpose of inter-comparison (Guan et al. 2011). For those regions with a pronounced single annual cycle (power spectra of single annual cycle >0.8), a sinusoid function,

$$T(t) = \bar{T} + A\cos(2\pi t - \theta) \quad (1)$$

is fitted to the time series $T(t)$ to estimate the

optimal parameters \bar{T} , A and θ simultaneously using the trust-region-reflective algorithm (Coleman and Li 1994, 1996), where \bar{T} refers to the mean value, A the magnitude of variation, and θ the phase.

2. *Correlation analysis*.—Spearman correlation coefficients were calculated between the time series of vegetation indices in order to investigate their consistency. Spearman correlations coefficients were also calculated between the time series of vegetation indices and environmental drivers.

3. *Hovmöller diagram*.—Hovmöller diagrams (longitudinal averages) are used to characterize the mean seasonal cycle along a latitude range. We focus on a typical tropical transect averaged over 1 degree in longitude (20° E–21° E) and spanning 30 degrees in latitude (10° N–20° S), with exclusion of pixels belonging to wetland. The pattern of Hovmöller diagrams shown here is only weakly dependent on the longitude because the Hovmöller diagrams centering on any of the longitudes from 19° E to 28° E show a similar seasonality (see Appendix B: Fig. B5). For better visual illustration, we show the Hovmöller diagrams of both the percentile value and the Hovmöller diagrams based on the data raw values.

RESULTS

Power spectra and phase analysis

From the power spectra and phase analysis, we find that deciduous forests and woodland in Africa almost all have pronounced single annual cycles, shown from both ORS and MVRS data (only single annual cycle of EVI and Ku-dB are shown in Fig. 2, power spectra of other datasets

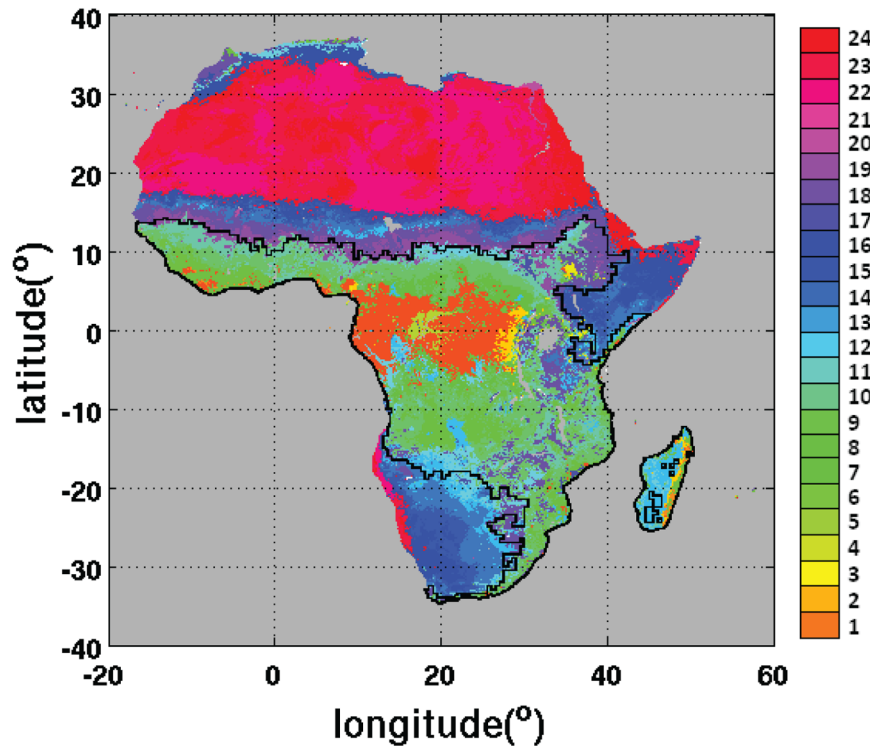


Fig. 1. Dominant land cover types from GLC2000 Africa product (1, Closed evergreen lowland forest; 2, Degraded evergreen lowland forest; 3, Submontane forest; 4, Montane forest; 5, Swamp forest; 6, Mangrove; 7, Mosaic Forest/Croplands; 8, Mosaic Forest/Savanna; 9, Closed deciduous forest; 10, Deciduous woodland; 11, Deciduous shrubland with sparse trees; 12, Open deciduous shrubland; 13, Closed grassland; 14, Open grassland with sparse shrubs; 15, Open grassland; 16, Sparse grassland; 17, Swamp bushland and grassland; 18, Croplands (>50%); 19, Croplands with open woody vegetation; 20, Irrigated croplands; 21, Tree crops; 22, Sandy desert and dunes; 23, Stony desert; 24, Bare rock). The black line indicates regions where annual mean LAI large than one.

are provided in Appendix B: Fig. B2). The phase information for the single annual cycle regions from EVI and Ku-dB are consistent with each other, with gradients in south-to-north direction in both northern Africa and southern Africa. This power spectra/phase pattern of vegetation is consistent with that of precipitation (Fig. 2), indicating that water is the dominating controlling factor for vegetation seasonality in African tropical deciduous forests and woodlands. However, this does not rule out the possibility that some tropical dry forests may flush their leaves slightly before the rainy season starts because remote sensing can only capture the large-scale pattern rather than taxonomic heterogeneity in phenology. The spectra and phase pattern of SWCNP and SWTOA are very different from those of EVI and Ku-dB in tropical deciduous

forests and woody savanna regions, indicating that SWCNP and SWTOA have little control on vegetation seasonality in these regions.

The situation in the tropical evergreen forest regions (3° N– 7° S) is more complex. Both EVI and Ku-dB have weaker single annual cycles, and relatively strong double annual cycles in this region (Fig. 2). EVI and precipitation have more similar spatial patterns for the power spectra of double annual cycles, and both are different from Ku-dB, with the largest differences shown in the northwestern part of tropical evergreen forests (i.e., Gabon and Cameroon).

Correlation analysis

Correlation analysis shows that EVI and Ku-dB are strongly positively correlated in tropical deciduous forests and woodlands, but they are

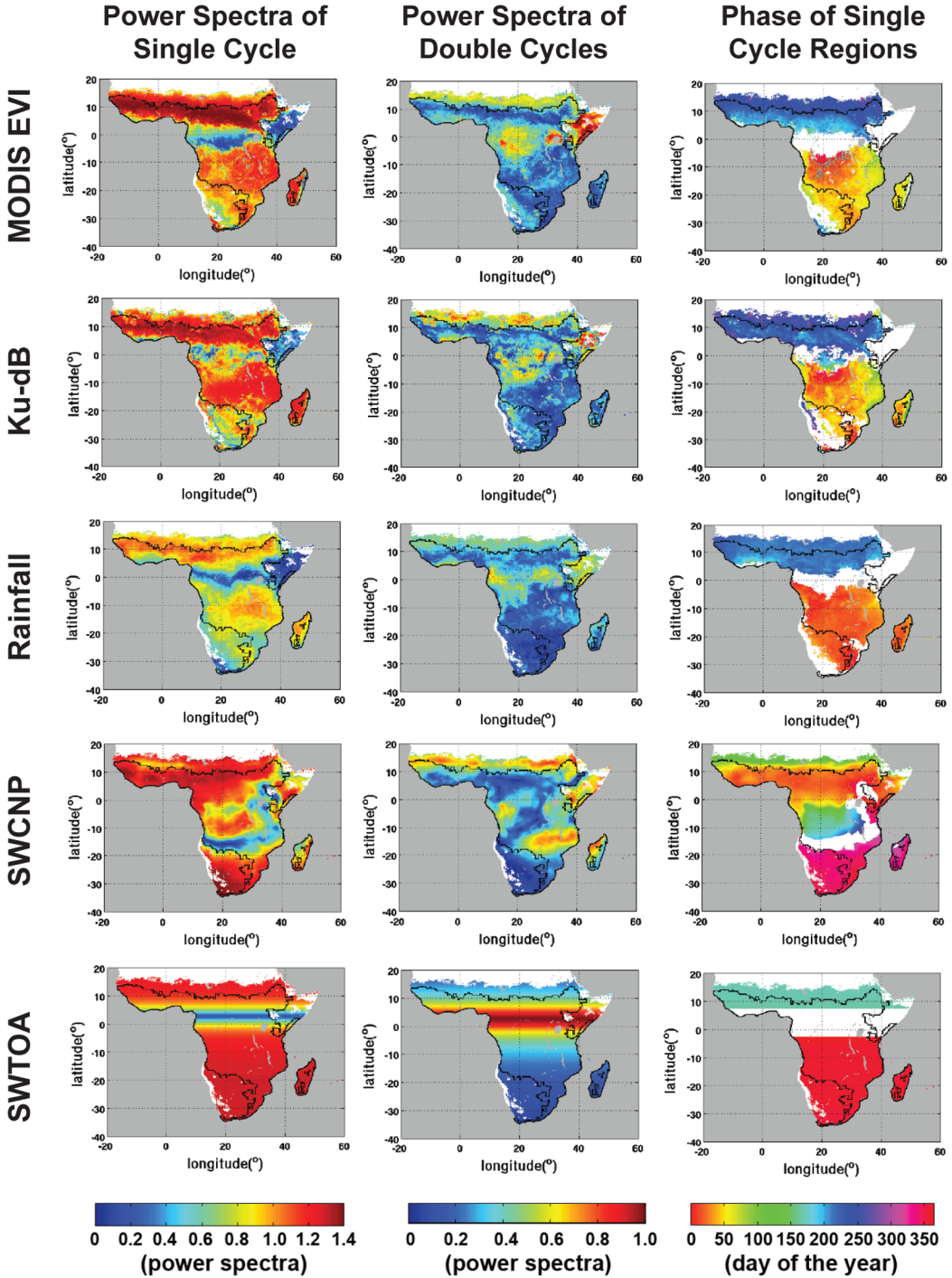


Fig. 2. The power spectra of single annual cycle (first column) and double annual cycles (second column) for the normalized time series of MODIS EVI, Ku-dB, precipitation, SWCNP and SWTOA. For those regions with pronounced single annual cycle (power spectra of annual cycle >0.8), a sinusoid function $T(t)=\bar{T} + A\cos(2\pi t - \theta)$ is fitted to the time series to estimate the optimal parameters \bar{T} , A and θ simultaneously. The phase information θ of the corresponding datasets are shown in the third column. The black line indicates regions where mean LAI large than one.

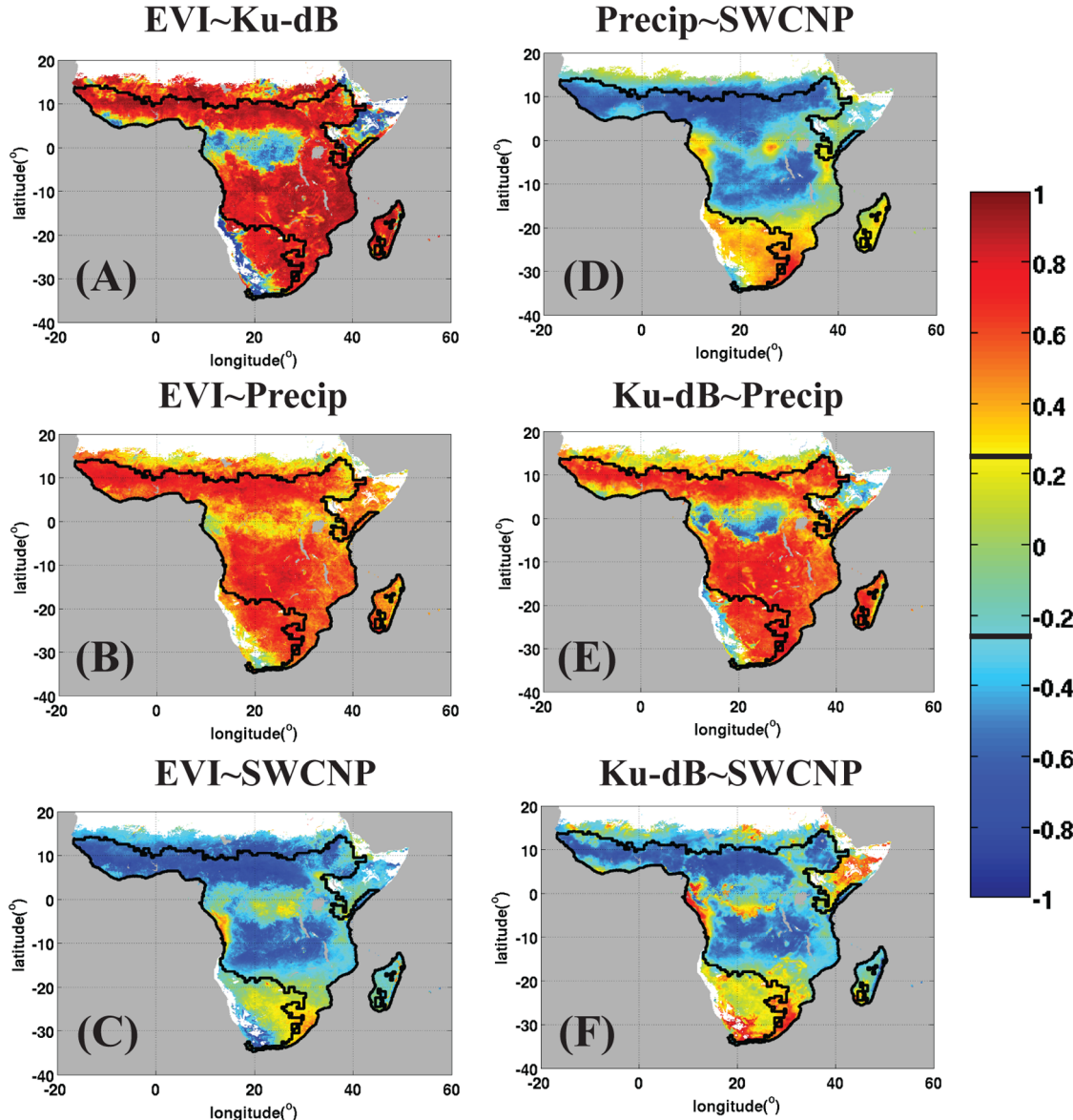


Fig. 3. Spearman Correlation coefficients of mean annual cycles between: (A) EVI and Ku-dB; (B) EVI and precipitation; (C) EVI and SWCNP; (D) precipitation and SWCNP; (E) Ku-dB and precipitation; (F) Ku-dB and SWCNP. Correlation coefficients greater than 0.24 or less than -0.24 satisfy the significance level of $P < 0.1$, which has been identified as the black lines in the colorbar.

uncorrelated or negatively correlated in tropical evergreen forests (Fig. 3A). Clear boundaries in Fig. 3A distinguish these two different regimes, which match well with the land-cover delineations of tropical evergreen and deciduous forests. EVI is highly correlated with precipitation almost over the whole tropical African region (Fig. 3B).

But Ku-dB shows significantly negative correlation with precipitation in evergreen forests (Fig. 3E). The seasonal coupling between EVI and Ku-dB in deciduous forest and woodland regions has been further illustrated in Fig. 4, where both EVI and Ku-dB have a high positive correlation with precipitation seasonality from latitude north of 5°

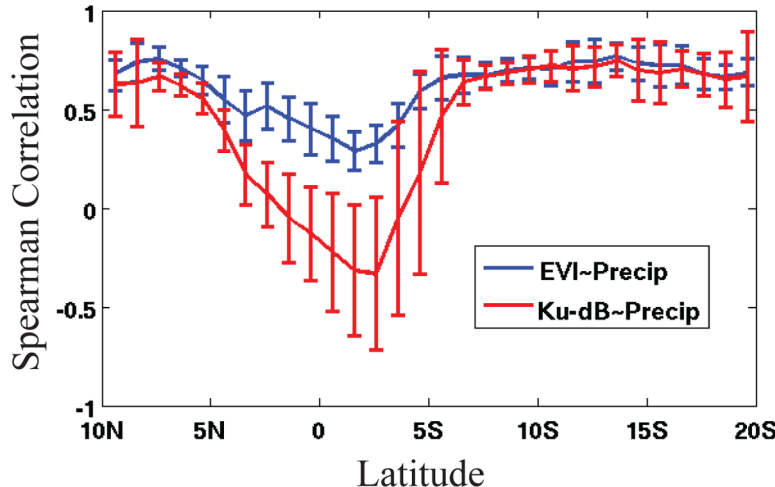


Fig. 4. Longitudinally-aggregated (20° E– 30° E) Spearman Correlation coefficients of mean annual cycle for EVI and precipitation (blue line) and Ku-dB and precipitation (red line), across the latitude from 10° N to 20° S. The error bars show the standard deviations of Spearman Correlation within each longitude bin (2°).

N and south of 7° S. This coupling breaks down for tropical evergreen forest regions (between 5° N and 7° S), where Ku-dB and EVI show almost reversed correlations with precipitation. We also find that SWCNP is negatively correlated with both EVI and Ku-dB in almost all of tropical Africa, except for parts of the tropical evergreen forest.

Hovmöller diagram

The Hovmöller diagrams of mean annual cycle of different datasets are shown in Fig. 5 (two mean annual cycles are put together for a better visual illustration). We find that EVI generally follows the precipitation seasonality for all the tropical regions ranging from 10° N– 20° S (the same for GIMMS-NDVI in Appendix B: Fig. B3). Ku-dB, EVI and precipitation are in phase in tropical deciduous forests and woody savanna regions (from 10° N– 5° N and 10° S– 20° S). But from the latitude of 3° N to 5° S (Fig. 5, second column for enlarged illustrations), there are pronounced phase shifts between Ku-dB and EVI. The regions of 5° N– 3° N and 5° S– 10° S exhibit a transitional state from in-phase to out-of-phase between the two data sets. Two MVRS datasets (Ku-dB and C-dB) share the similar spatial pattern in the Hovmöller diagram (Appendix B: Fig. B3), with C-dB showing less

temporal variability in the tropics due to its larger wavelength having less sensitivity to leaf biomass and leaf water content.

For tropical evergreen forest regions (3° N– 5° S), SWTOA behaves as a precursor of Ku-dB, i.e., the two insolation maximum peaks correspond to the rising times of Ku-dB from the two bottoms in its seasonal evolution. The latitudinal shifts of Ku-dB and insolation are in the same direction for the two cycles over the course of a year.

We also find that SWCNP is out of phase with both EVI and Ku-dB almost across the whole tropical range 10° N– 20° S. Seasonality patterns of day-length, sunrise, and sunset (Fig. 5) cannot explain the continuous equatorial transitions in either EVI or Ku-dB.

DISCUSSION

The results show that the seasonalities of ORS and MVRS data are strongly coupled in tropical deciduous forest and woody savannas, which are mainly controlled by precipitation. Fig. 6A and C shows two typical examples of this case (i.e., the time series of interested variables at 10.5° N and 15.5° S, respectively), which clearly demonstrate the precipitation controls on both EVI and Ku-dB trajectories.

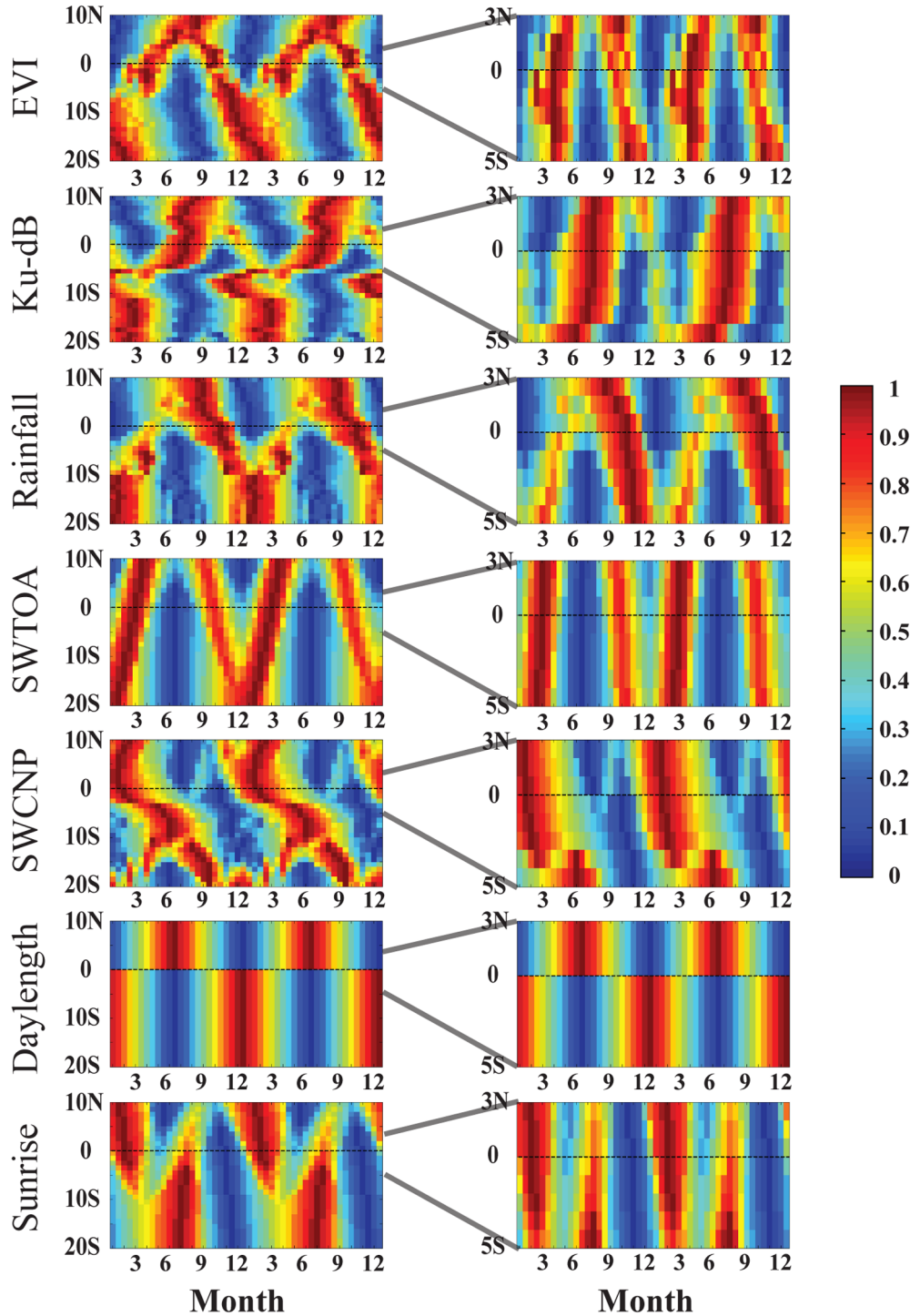


Fig. 5. First column: Hovmöller diagrams of mean annual cycle with percentile (or rank) values across the latitude from 10° S to 20° N for: EVI, Ku-dB, rainfall, SWTOA, SWCNP, day-length and sunrise. All the Hovmöller diagrams are averaged for the pixels from 20° E to 21° E in longitude. Second column: enlarged Hovmöller diagrams of mean annual cycle with percentile (or rank) values for the latitude from 3° S to 5° N for the same set of variables.

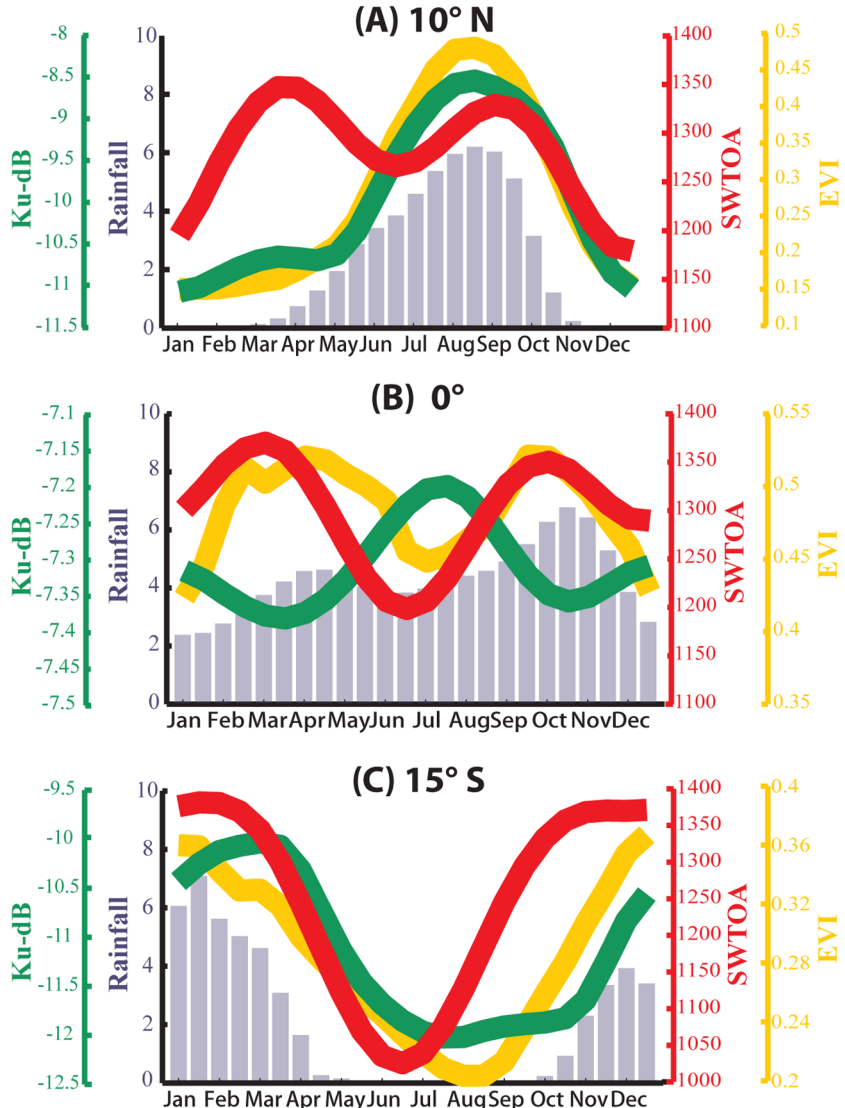


Fig. 6. Mean annual time series of the interested variables for: (A) 10° N; (B) 0°; and (C) 15° S. The variables shown includes: EVI, Ku-dB (unit: dB), precipitation (unit: mm/day), and SWTOA at noon (unit: W/m²). The mean annual time series are averaged for a square area with latitude width of 1° (centering at 10° N, 0° S, and 15° S, respectively), and with longitude width of 1° (all centering at 20.5° E).

We find that the seasonality of tropical evergreen forest is weak but exists. ORS and MVRS data show very different seasonality patterns, though both of them have double annual cycles. ORS follows precipitation seasonality in general. Ku-dB data start to rise from minimum values synchronous with the maximum SWTOA (see Fig. 6B), and this correspondent pattern between Ku-dB and SWTOA

persists in the tropical evergreen forest regions from 3° N to 5° S (Fig. 5).

SWCNP, day-length, sunrise or sunset variations cannot be attributed as controls on the seasonal evolution of either EVI or Ku-dB. In the tropical Amazon, both radiation and cloudiness have been proposed as candidates of controlling the vegetation seasonal evolution (Saleska et al. 2003, Myneni et al. 2007, Betts and Dias 2010,

Bradley et al. 2011), but this is not the case in tropical Africa. Our recent work has found that tropical evergreen forests in Africa have much less wet-season rainfall than their counterparts in the Amazon and Asian islands. This constrains the water storage which can be carried over from wet seasons to dry seasons, and limits the physiological functioning of African tropical forests during the dry season. Thus vegetation functions (e.g., photosynthetic activity or transpiration) follow precipitation rather than other environmental variables.

The different physical properties captured by ORS and MVRS data can explain their distinctive behaviors in tropical evergreen and deciduous forests. ORS represents landscape-integrated vegetation photosynthetic capacity depending on both vegetation fractional cover and leaf photochemical attributes (e.g., chlorophyll content), and leaf photochemical attributes is further determined by both leaf area and leaf-level photosynthetic capacity. For tropical deciduous forests and woody savannas, seasonality of leaf area/biomass and leaf-level photosynthetic activity usually co-vary, i.e., deciduous trees can only have photosynthesis and transpiration when leaves are present. Thus, ORS captures the multiplicative feature of leaf area and leaf-level photosynthetic activity (Guan et al. 2012). However, for tropical evergreen forests characterized with closed canopy, ORS has little sensitivity to leaf area due to the very high leaf biomass throughout the year. The seasonality in ORS is mostly attributed to variation in canopy-level leaf biochemical properties, which strongly tie to plant photosynthetic activity. This can explain why the seasonality of ORS follows precipitation in the tropical evergreen forests, since the soil moisture deficit limits the photosynthetic activities during dry seasons, given that African evergreen forests are still water-limited in general. It is also worth noting that all the ORS data show the similar pattern including an LAI product from SEVERI (Appendix B: Fig. B3). Currently most satellite LAI products are derived from VI or similar reflectance ratios based on visible and NIR spectra. How to interpret these derived LAI products in tropical evergreen forests requires caution because they may not be quantifying the actual leaf area (e.g., Doughty and Goulden 2008).

MVRS data (mainly valid for Ku-dB) represent leaf biomass and leaf water content for the top portion of the canopy, with contribution from soil moisture depending on soil fraction in a pixel. For tropical forests, soil moisture has little contribution for dB since little fraction of bare soil is in the scene (Frolking et al. 2011, Guan et al. 2012). Thus the dominating information of Ku-dB is from leaf biomass. For deciduous forests and woody savannas, leaf area/biomass co-varies with canopy-level photosynthetic activity; this explains why dB strongly correlates and also shares a similar seasonality with ORS in these regions. For tropical evergreen forests, dB, with more sensitivity to leaf biomass, characterizes the leaf phenological evolution to the largest extent.

This study is the first one to use remote sensing to test and confirm the field-based finding (Yeang 2007a, b) that insolation intensity controls tropical evergreen vegetation, i.e., the double annual cycles of leaf-flushing in tropical evergreen forest are synchronous with the annual bi-model insolation intensity. The SWTOA-dB feature is only found at 3° N–5° S because in this range the vegetation types are homogenously tropical evergreen forests (we exclude wetland pixels in our analysis). Beyond this range, tropical evergreen trees are mixed with more deciduous trees, where the microwave signal follows precipitation rather than SWTOA. Thus there is a transitional range beyond the homogenous tropical evergreen forest regions (3° N–5° S).

We interpret Ku-dB as the leaf biomass trajectory, which implies that leaf-flushing synchronizes with the insolation intensity peak. Since the SWTOA almost has no inter-annual variation, Ku-dB signals should also have little inter-annual variation at its two initiation points (corresponding to the two leaf-flushing times). We find there is little inter-annual variation in the Ku-dB initiation points given the noisy condition of dB in the tropics (results not shown here). We also observe that the double cycles of Ku-dB are asymmetric, with the cycle from April to September much stronger than the cycle from November to January. This also confirms the field-based finding by Yeang (2007b), who attributed the unequal solar radiation received at the ground to the cloud covers in these two periods. It is worth noting that there are

relatively large uncertainties related to Ku-dB data in the tropical evergreen forests as shown in Appendix B: Fig. B1. We argue that the spatial pattern of Ku-dB after the smoothing approach reveals a continuous spatial structure rather than some spatially random patterns, which implies the existence of an underlying structure in the Ku-dB signals.

Conclusion

In this paper, the seasonality of vegetation functions (i.e., canopy photosynthesis capacity) and structure (i.e., canopy leaf biomass changes) in African tropical forests is investigated using multiple remote sensing datasets from optical and microwave sensors. The results reveal a strong seasonality coupling between vegetation function and structure for tropical deciduous forests and woody savannas, which is controlled by precipitation. Shortwave radiation at the top of canopy, day-length, sunrise or sunset variations have limited control on the seasonal evolution of tropical forests in Africa. For African tropical evergreen forests, seasonality decoupling of vegetation functions and structures are discovered from optical and microwave sensors. Canopy photosynthetic activity observed by ORS follows precipitation seasonality due to the deficit of soil moisture limiting plant biochemical activity during dry seasons. Canopy-top leaf biomass inferred from Ku-dB exhibits two leaf-flushings over a year, synchronous with the two peaks in insolation intensity, consistent with field observations. A pan-tropical analysis across the world with optical and microwave data is worth conducting to reveal a complete picture of tropical forest phenological patterns and their controls. We further suggest more field campaigns to collect large-scale tropical evergreen forest phenology information in the pan-tropics to verify our findings.

ACKNOWLEDGMENTS

We greatly appreciate all the data providers for their generosity of sharing datasets for scientific research. We are also grateful for the computational support provided by the PICSciE-OIT High Performance Computing Center at Princeton University. The Subject-matter Editor Dr. Epstein and anonymous reviewers provided constructive suggestions and comments to significantly improve the manuscript. Dr. Damien

Garcia generously provided the smoothing algorithm with the calculation of confidence interval. K. Guan and E. F. Wood are supported by the NASA grant NNX08AL59G and NASA NESSF fellowship. K. K. Caylor is supported by the NSF grants EAR-847368 and BCS/ESE-1026334.

LITERATURE CITED

- Betts, A. K. and M. A. F. S. Dias. 2010. Progress in understanding land-surface-atmosphere coupling from LBA research. *Journal of Advanced Modeling Earth Systems* 2:6.
- Bonan, G. 2008. Ecological climatology: concepts and applications. Second edition. Cambridge University Press, Cambridge, UK.
- Borchert, R. 1998. Response of tropical trees to rainfall seasonality and its long-term changes. *Climatic Change* 39:381–393.
- Borchert, R., S. S. Renner, Z. Calle, D. Navarrete, A. Tye, L. Gautier, R. Spichiger, and P. von Hildebrand. 2005. Photoperiodic induction of synchronous flowering near the equator. *Nature* 433:627–629.
- Bradley, A. V., F. F. Gerard, N. Barbier, G. P. Weedon, L. O. Anderson, C. Huntingford, L. E. O. C. Araújo, P. Zelazowski, and E. Ara. 2011. Relationships between phenology, radiation and precipitation in the Amazon region. *Global Change Biology* 17:2245–2260.
- Calle, Z., B. O. Schlumpberger, L. Piedrahita, A. Leftin, S. A. Hammer, A. Tye, and R. Borchert. 2010. Seasonal variation in daily insolation induces synchronous bud break and flowering in the tropics. *Trees* 24:865–877.
- Calle, Z., A. H. Strahler and R. Borchert. 2009. Declining insolation induces synchronous flowering of Montanoa and Simsia (Asteraceae) between Mexico and the Equator. *Trees* 23:1247–1254.
- Chambers, J. Q., G. P. Asner, D. C. Morton, L. O. Anderson, S. S. Saatchi, F. D. Espírito-Santo, M. Palace, and C. Souza, Jr. 2007. Regional ecosystem structure and function: ecological insights from remote sensing of tropical forests. *Trends in Ecology and Evolution* 22(8):414–423.
- Coleman, T., and Y. Li. 1994. On the convergence of reflective newton methods for large- scale nonlinear minimization subject to bounds. *Mathematical Programming* 67(2):189–224.
- Coleman, T., and Y. Li. 1996. An interior, trust region approach for nonlinear minimization subject to bounds. *SIAM Journal on Optimization* 6:418–445.
- Dawson, T. E. 1996. Determining water use by trees and forests from isotopic, energy balance and transpiration analyses: the roles of tree size and hydraulic lift. *Tree Physiology* 16:263–272.
- Doughty, C. E., and M. L. Goulden. 2008. Seasonal

- patterns of tropical forest leaf area index and CO₂ exchange. *Journal of Geophysical Research* 113:G00B06.
- Dirzo, R. and P. H. Raven. 2003. Global state of biodiversity and loss. *Annual Review of Environment and Resources* 28:137–167.
- Elliott, S., P. J. Baker, and R. Borchert. 2006. Leaf flushing during the dry season: the paradox of Asian monsoon forests. *Global Ecology and Biogeography* 15(3):248–257.
- Fisher, J. B. et al. 2009. The land-atmosphere water flux in the tropics. *Global Change Biology* 15(11):2694–2714.
- Frolking, S., S. Hagen, T. Milliman, M. Palace, J. Z. Shimbo, and M. Fahnestock. 2012. Detection of large-scale forest canopy change in pan-tropical humid forests 2000–2009 with the SeaWinds Ku-Band Scatterometer. *IEEE Transactions on Geoscience and Remote Sensing* 50(7):2603–2617.
- Frolking, S., M. Fahnestock, T. Milliman, K. McDonald, and J. Kimball. 2005. Interannual variability in North American grassland biomass/productivity detected by SeaWinds scatterometer backscatter. *Geophysical Research Letters* 32:L21409.
- Frolking, S., T. Milliman, K. McDonald, J. Kimball, M. Zhao, and M. Fahnestock. 2006. Evaluation of the SeaWinds scatterometer for regional monitoring of vegetation phenology. *Journal of Geophysical Research* 111:D17302.
- Frolking, S., T. Milliman, M. Palace, D. Wisser, R. Lammers, and M. Fahnestock. 2011. Tropical forest backscatter anomaly evident in SeaWinds scatterometer morning over-pass data during 2005 drought in Amazonia. *Remote Sensing of Environment* 115:897–907.
- Glenn, E. P., A. R. Huete, P. L. Nagler, and S. G. Nelson. 2008. Relationship between remotely-sensed vegetation indices, canopy attributes and plant physiological processes: what vegetation indices can and cannot tell us about the landscape. *Sensors* 8:2136–2160.
- Garcia, D. 2010. Robust smoothing of gridded data in one and higher dimensions with missing values. *Computational Statistics and Data Analysis* 54:1167–1178.
- Garcia-Haro, F. J., F. C. de Coca, and J. Meli. 2008. Product user manual (PUM): vegetation parameters (FVC, LAI, FAPAR). Technical Report. Land SAF Project.
- Guan, K., S. E. Thompson, C. J. Harman, N. B. Basu, P. S. C. Rao, M. Sivapalan, A. I. Packman, and P. K. Kalita. 2011. Spatiotemporal scaling of hydrological and agrochemical export dynamics in a tile-drained Midwestern watershed. *Water Resource Research* 47:W00J02.
- Guan, K., E. F. Wood, and K. K. Caylor. 2012. Multi-sensor derivation of regional vegetation fractional cover in Africa. *Remote Sensing of Environment* 124:653–665.
- Hallé, F., R. A. A. Oldeman, and P. B. Tomlinson. 1978. *Tropical trees and forests: an architectural analysis*. Springer, New York, New York, USA.
- Hardin, P. J., and M. W. Jackson. 2003. Investigating SeaWinds terrestrial backscatter: Equatorial savannas of South America. *Photogrammetric Engineering and Remote Sensing* 69(11):1243–1254.
- Huete, A., K. Didan, T. Miura, E. Rodriguez, X. Gao, and L. Ferreira. 2002. Overview of the radiometric and biophysical performance of the MODIS vegetation indices. *Remote Sensing of Environment* 83:195–213.
- Huete, A., N. Restrepo-Coupe, P. Ratana, K. Didan, S. Saleska, K. Ichii, S. Panuthai, and M. Gamo. 2008. Multiple site tower flux and remote sensing comparisons of tropical forest dynamics in Monsoon Asia. *Agricultural and Forest Meteorology* 148:748–760.
- Huffman, G. J., D. T. Bolvin, E. J. Nelkin, D. B. Wolff, R. F. Adler, K. P. Bowman, and E. F. Stocker. 2007. The TRMM Multisatellite Precipitation Analysis (TMPA): Quasi-global, multiyear, combined-sensor precipitation estimates at fine scales. *Journal of Hydrometeorology* 8:38–55.
- Jackson, S. D. 2009. Plant responses to photoperiod. *New Phytologist* 181:517–531.
- Jarlan, L., E. Mougin, P. Frison, P. Mazzeg, and P. Hiernaux. 2002. Analysis of ERS wind scatterometer time series over Sahel (Mali). *Remote Sensing of Environment* 81:404–415.
- Jensen, J. R. 2000. *Remote sensing of the environment: an earth resource perspective*. Pearson Prentice-Hall, Upper Saddle River, New Jersey, USA.
- Kim, Y., R. G. Knox, M. Longo, D. Medvigy, L. R. Hutyra, E. H. Pyle, S. C. Wofsy, R. L. Bras, and P. R. Moorcroft. 2012. Seasonal carbon dynamics and water fluxes in an Amazon rainforest. *Global Change Biology* 18(4):1322–1334.
- Long, D. 2001. BYU daily browse images of QuikSCAT Sigma-0 measurements. Technical Report. Brigham Young University, Provo, Utah, USA.
- Ma, Y. and R. T. Pinker. 2012. Modeling shortwave radiative fluxes from satellites. *Journal of Geophysical Research* 117:D23202.
- Markewitz, D., S. Devine, E. A. Davidson, P. Brando, and D. C. Nepstad. 2010. Soil moisture depletion under simulated drought in the Amazon: impacts on deep root uptake. *New Phytologist* 187:592–607.
- Mayaux, P. et al. 2003. A land cover map of Africa. Technical Report. EU Joint Research Center, Brussels, Belgium.
- Meir, P., P. M. Brando, D. Nepstad, S. Vasconcelos, A. C. L. Costa, E. Davidson, S. Almeida, R. A. Fisher, E. D. Sotta, D. Zarin, and G. Cardinot. 2009. The effects of drought on Amazonian rain forests.

- Pages 429–449 in M. Keller, M. Bustamante, J. Gash, and P. Silva Dias, editors. *Amazonia and global change*. World Scientific Publishing, Hackensack, New Jersey, USA.
- Meir, P. and F. I. Woodward. 2010. Amazonian rain forests and drought: response and vulnerability. *New Phytologist* 187(3):553–557.
- Myneni, R. B. et al. 2007. Large seasonal swings in leaf area of Amazon rainforests. *Proceedings of the National Academy of Sciences* 104(12):4820–4823.
- Nemani, R. R., C. D. Keeling, H. Hashimoto, W. M. Jolly, S. C. Piper, C. J. Tucker, R. B. Myneni, and S. W. Running. 2003. Climate-driven increases in global terrestrial net primary production from 1982 to 1999. *Science* 300:1560–1563.
- Nepstad, D. C., R. C. de Carvalho, E. A. Davidson, P. H. Jipp, P. A. Lefebvre, G. H. Negreiros, E. D. da Silva, T. A. Stone, S. E. Trumbore, and S. Vieira. 1994. The role of deep roots in the hydrological and carbon cycles of Amazonian forests and pastures. *Nature* 372:666–669.
- Pan, Y. et al. 2011. A large and persistent carbon sink in the world's forests. *Science* 333:988–993.
- Reich, P. 1995. Phenology of tropical forests: patterns, causes, and consequences. *Canadian Journal of Botany* 73:164–174.
- Reich, P. B. and R. Borchert. 1984. Water stress and tree phenology in a tropical dry forest in the lowlands of Costa Rica. *Journal of Ecology* 72(1):61–74.
- Renner, S. S. 2007. Synchronous flowering linked to changes in solar radiation intensity. *New Phytologist* 175:195–197.
- Richardson, A. D., T. F. Keenan, M. Migliavacca, Y. Ryu, O. Sonnentag, and M. Toomey. 2013. Climate change, phenology, and phenological control of vegetation feedbacks to the climate system. *Agricultural and Forest Meteorology* 169:156–173.
- Rivera, G., and R. Borchert. 2001. Induction of flowering in tropical trees by a 30-min reduction in photoperiod: evidence from field observations and herbarium specimens. *Tree Physiology* 21:201–212.
- Rivera, G., S. Elliott, L. S. Caldas, G. Nicolossi, V. T. R. Coradin, and R. Borchert. 2002. Increasing daylength induces spring flushing of tropical dry forest trees in the absence of rain. *Trees* 16:445–456.
- Saatchi, S. S., et al. 2011. Benchmark map of forest carbon stocks in tropical regions across three continents. *Proceedings of the National Academy of Sciences* 108(2):9899–9904.
- Saleska, S. R. et al. 2003. Carbon in Amazon forests: unexpected seasonal fluxes and disturbance-induced losses. *Science* 302:1554–1557.
- Saleska, S., H. da Rocha, B. Kruyt, and A. Nobre. 2009. Ecosystem carbon fluxes and Amazonian forest metabolism. Pages 389–407 in M. Keller, M. Bustamante, J. Gash, and P. Silva Dias, editors. Amazonia and global change. World Scientific Publishing, Hackensack, New Jersey, USA.
- Sellers, P. J. 1985. Canopy reflectance, photosynthesis and transpiration. *International Journal of Remote Sensing* 6(8):1335–1372.
- Sellers, P. J. 1987. Canopy reflectance, photosynthesis, and transpiration. II. The role of biophysics in the linearity of their interdependence. *Remote Sensing of Environment* 21:143–183.
- Sellers, P. J., J. A. Berry, G. J. Collatz, C. B. Field, and E. G. Hall. 1992. Canopy reflectance, photosynthesis, and transpiration. III. A reanalysis using improved leaf models and a new canopy integration scheme. *Remote Sensing of Environment* 42:187–216.
- Sitch, S. et al. 2008. Evaluation of the terrestrial carbon cycle, future plant geography and climate-carbon cycle feedbacks using five Dynamic Global Vegetation Models (DGVMs). *Global Change Biology* 14(9):2015–2039.
- Solano, R., K. Didan, A. Jacobson, and A. Huete. 2010. MODIS vegetation index users guide. Collection 5. Vegetation Index and Phenology Lab, University of Arizona, Tucson, Arizona, USA.
- Toan, T. L., A. Beaudoin, J. Riou, and D. Guyon. 1992. Relating forest biomass to SAR data. *IEEE Transactions on Geoscience and Remote Sensing* 30(2):403–411.
- Tucker, C. J., J. E. Pinzon, and M. E. Brown. 2003. GIMMS NDVI user guide. Technical Report. Global Land Cover Facility, University of Maryland, College Park, Maryland, USA.
- Tucker, C. J., J. E. Pinzon, M. E. Brown, D. A. Slayback, E. W. Pakal, R. Mahoney, E. F. Vermote, and N. E. Saleous. 2005. An extended AVHRR 8-km NDVI dataset compatible with MODIS and SPOT vegetation NDVI data. *International Journal of Remote Sensing* 26(20):4485–4498.
- Ulaby, F., R. Moore, and A. Fung. 1982. Microwave remote sensing: active and passive. Volume 2: Radar remote sensing and surface scattering and emission theory. Addison-Wesley, Reading, Massachusetts, USA.
- van Schaik, C. P., J. W. Terborgh, and S. J. Wright. 1993. The phenology of tropical forests: Adaptive significance and consequences for primary consumers. *Annual Review of Ecology and Systematics* 24:353–377.
- Waring, R. H., J. Way, E. R. Hunt, Jr., L. Morrissey, K. J. Ranson, J. F. Weishampel, R. Oren, and S. E. Franklin. 1995. Imaging radar for ecosystem studies. *BioScience* 45(10):715–723.
- Williams, L. J., S. Bunyavejchewin, and P. J. Baker. 2008. Deciduousness in a seasonal tropical forest in western Thailand: interannual and intraspecific variation in timing, duration and environmental cues. *Oecologia* 155:571–582.

- Williams, R. J., B. A. Myers, W. J. Muller, G. A. Duff, and D. Eamus. 1997. Leaf phenology of woody species in a north Australian tropical savanna. *Ecology* 78:2542–2558.
- Wright, S. J., and C. P. van Schaik. 1994. Light and the phenology of tropical trees. *American Naturalist* 143(1):192–199.
- Yeang, H.-Y. 2007a. Synchronous flowering of the rubber tree (*Hevea brasiliensis*) induced by high solar radiation intensity. *New Phytologist* 175(2):283–289.
- Yeang, H.-Y. 2007b. The sunshine-mediated trigger of synchronous flowering in the tropics: the rubber tree as a study model. *New Phytologist* 176:730–735.

SUPPLEMENTAL MATERIAL

APPENDIX A

Table A1. Abbreviations and explanations used in the paper.

Abbreviation	Explanation
AVHRR	Advanced Very High Resolution Radiometer
ERS	European Remote-Sensing
ESA	European Space Agency
ET	Evapotranspiration
LAI	Leaf Area Index
GIMMS	Global Inventory Modeling and Mapping Studies
GISS	Goddard Institute for Space Studies
GLC2000	Global Land Cover mapping for the year 2000
GPP	Gross Primary Production
MEaSUREs	NASA program “Making Earth System Data Records for Use in Research Environments”
MVRS	Microwave Remote Sensing
MODIS	Moderate-resolution Imaging Spectroradiometer
MSG	Meteosat Second Generation
NASA	National Aeronautics and Space Administration
NDVI	Normalized Difference Vegetation Index
ORS	Optical Remote Sensing
SEVERI	Spinning Enhanced Visible and Infrared Imager
SWCNP	Shortwave downward radiation at the top of canopy; here it is equivalent to the shortwave downward radiation on the surface
SWTOA	Shortwave downward radiation at the top of atmosphere; here it is equivalent to the insolation intensity at the top of atmosphere
TRMM	Tropical Rainfall Measuring Mission

APPENDIX B

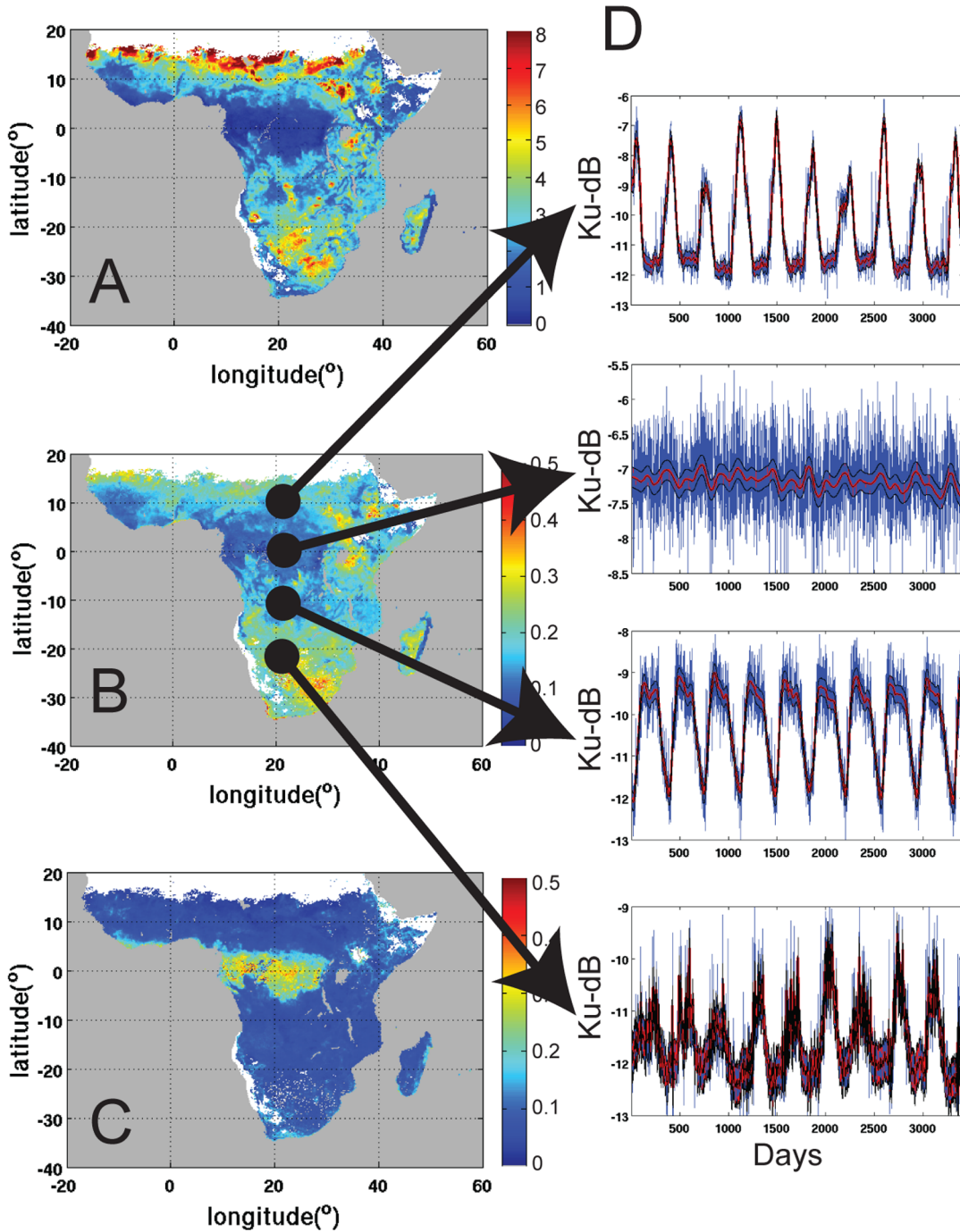


Fig. B1. (A) Mean magnitude of annual cycles of Ku-dB (maximum value minus minimum value for a year) at per-pixel level; (B) 99% confidence interval value of smoothed dB after applied the robust smooth algorithm (Garcia 2010) at the per pixel level, which provides a quantitative characterization of the uncertainties of the smoothed Ku-dB time series; (C) ratio of (B) over (A), which shows that the Ku-dB in equatorial Africa contains relatively more uncertainties than Ku-dB in other regions; (D) some typical examples of different latitudes (longitudes are all fixed at 20° E; latitudes are 10° S, 0°, 10° N, and 20° N).

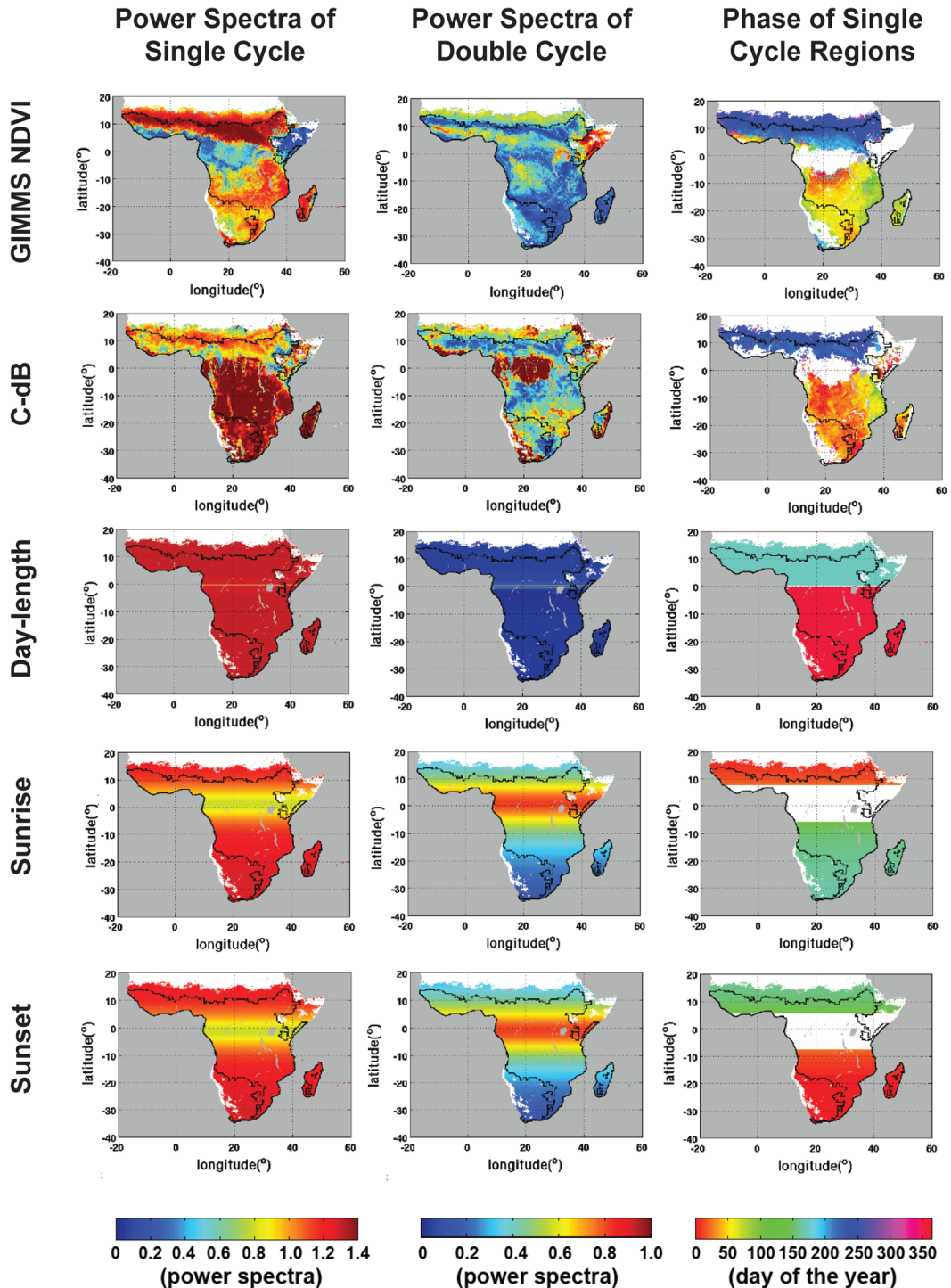


Fig. B2. The power spectra of single annual cycle (first column) and double annual cycles (second column) for the normalized time series of: GIMMS NDVI, C-dB, day-length, sunrise and sunset. For those regions with pronounced single annual cycle (power spectra of single annual cycle >0.8), a sinusoid function $T(t) = \bar{T} + A\cos(2\pi t - \theta)$ is fitted to the time series to estimate the optimal parameters \bar{T} , A and θ simultaneously. The phase information θ of the corresponding datasets are shown in the third column.

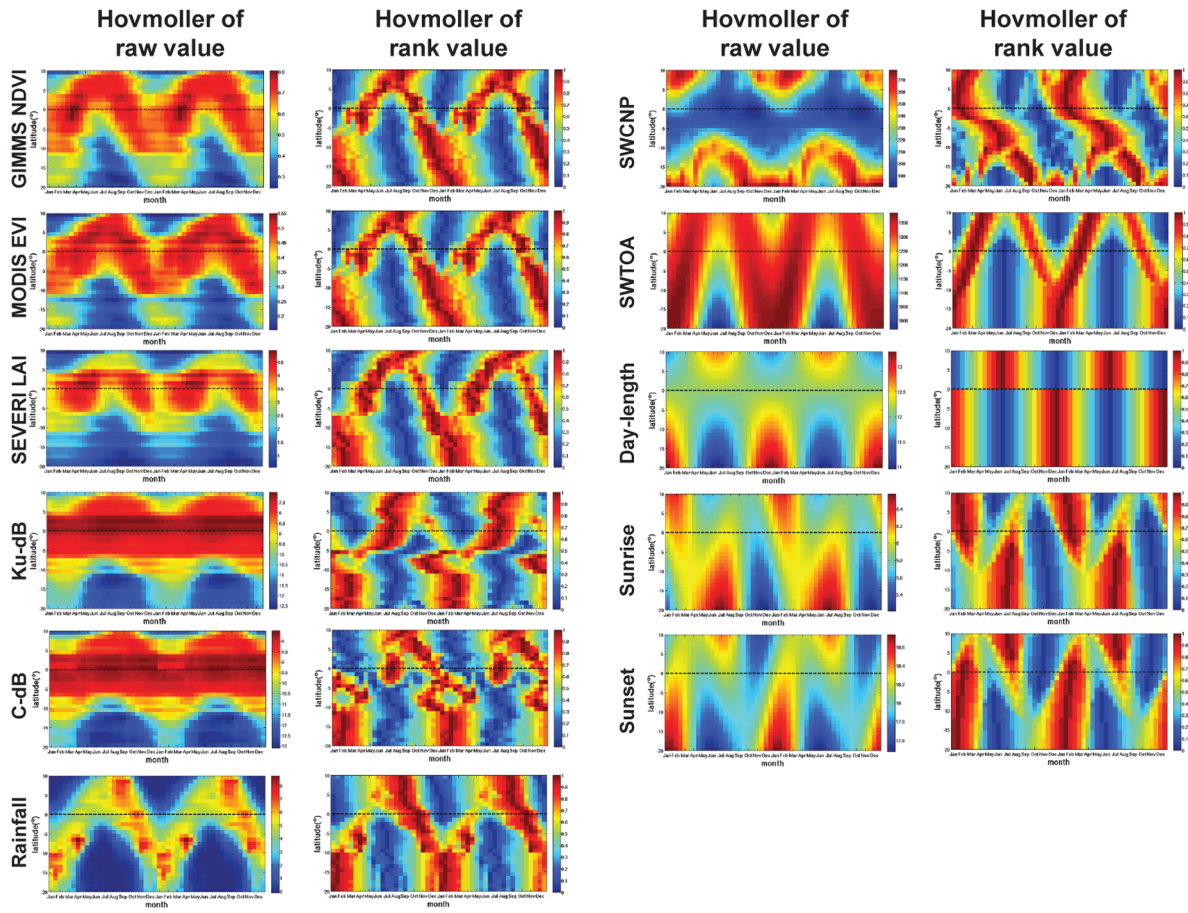


Fig. B3. Hovmöller diagrams of mean annual cycle with raw values (first column) and percentile/rank values (second column) for: GIMMS NDVI, MODIS EVI, Ku- dB (dB), C-dB (dB), rainfall (mm/day), SWCNP (W/m^2), SWTOA at noon (W/m^2), day-length (hours), sunrise (hour of the day) and sunset (hour of the day). All the Hovmöller diagrams are based on transect across the latitude from 10° S to 20° N, averaging at the longitude from 20° E to 21° E.

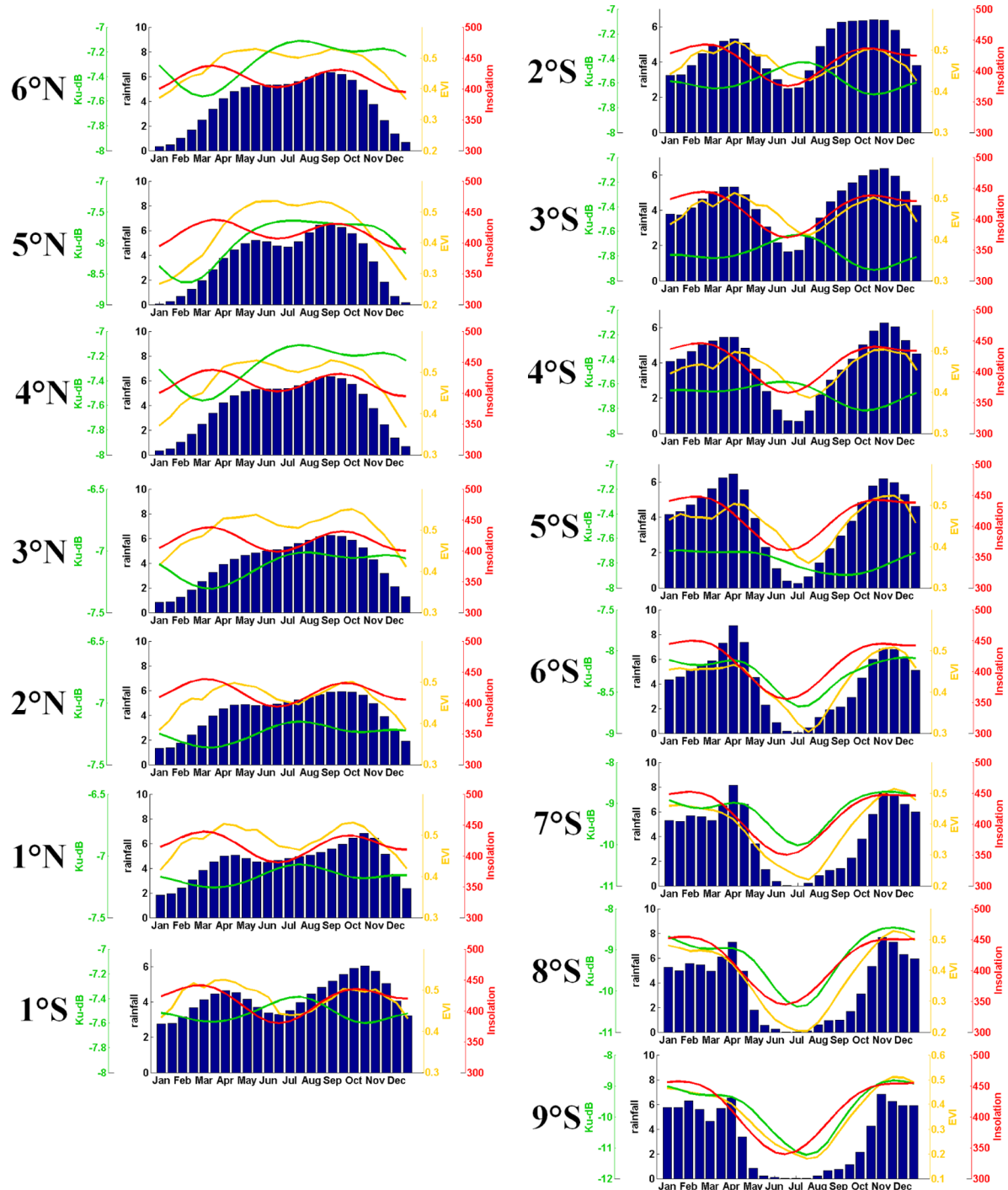


Fig. B4. Mean annual time series of the interested variables across the different latitudes from 6° N to 9° S. The variables shown includes: EVI, Ku-dB (dB), precipitation (mm/day), and daily mean SWTOA (W/m^2). The mean annual time series are averaged for a square area with latitude width of 1° (centering at the latitudes from 6° N to 9° S), and with longitude width of 1° (all centering at 20.5° E).

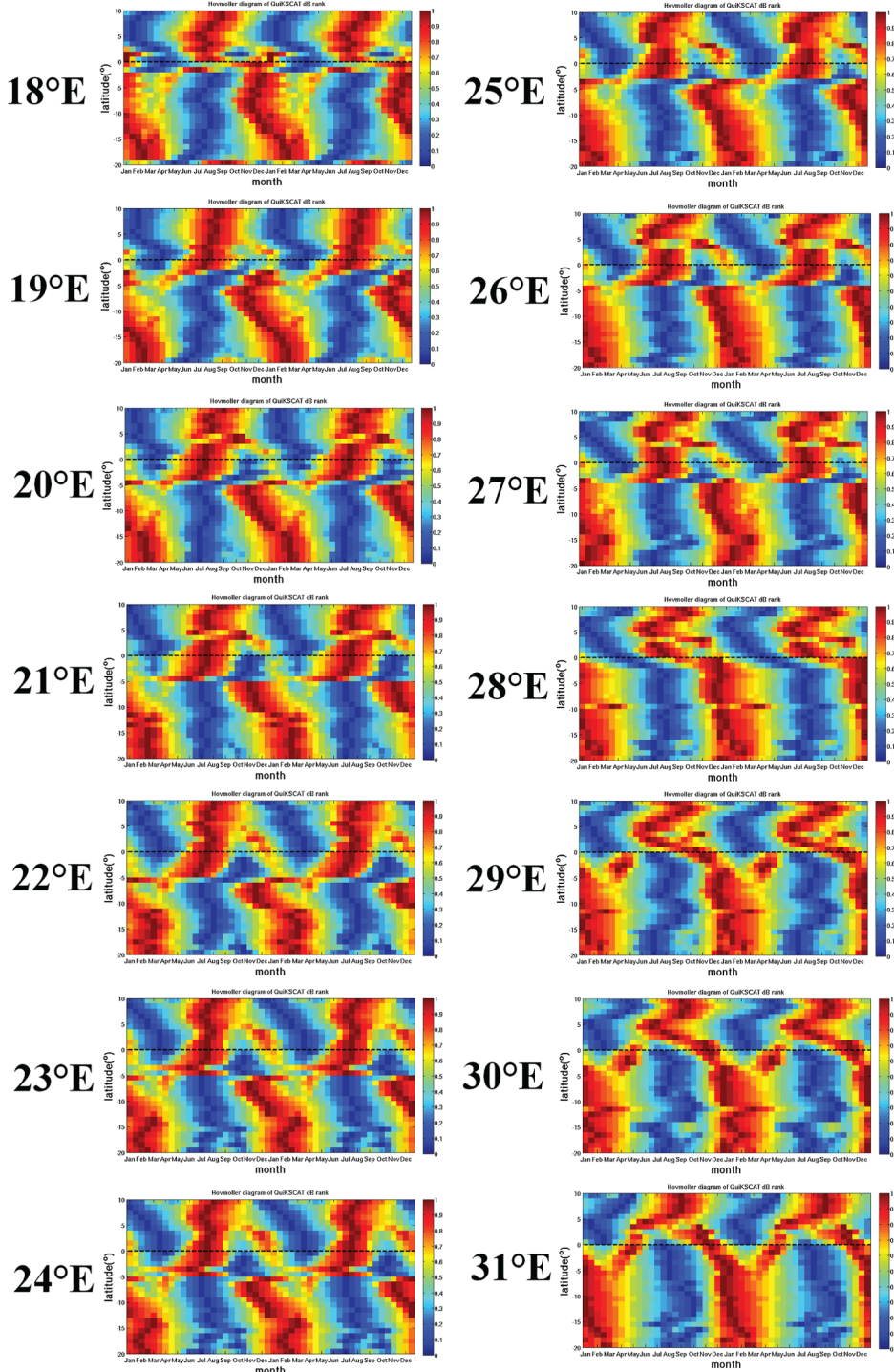


Fig. B5. Hovmöller diagrams of mean annual cycle with percentile (or rank) for Ku-dB from QuikSCAT (2000–2009). All the Hovmöller diagrams are based on transects across the latitude from 10° S to 20° N, but the longitudes vary from 18° E to 31° E. Hovmöller diagrams from 19° E to 27° E show similar patterns for vegetation seasonality as we discussed in the paper for Ku-dB over tropical evergreen forests, and these regions are also homogenous tropical evergreen forest regions.